Locating sources of volcanic tremor and emergent events by seismic triangulation: Application to Arenal volcano, Costa Rica

Jean-Philippe Métaxian, Philippe Lesage, Bernard Valette

Locating sources of volcanic tremor and emergent events by seismic triangulation: Application to Arenal volcano, Costa Rica

Jean-Philippe Métaxian,[1] Philippe Lesage,[2] and Bernard Valette[1]
Laboratoire de Géophysique Interne et Tectonophysique, Université de Savoie, Le Bourget-du-Lac, France

Received 16 April 2001; revised 3 April 2002; accepted 12 April 2002; published 23 October 2002.

[1] We address the issue of locating the sources of volcanic tremor and emergent events with a method requiring a limited amount of equipment. A network of several triangular seismic antennas made of vertical sensors is used. The slowness vectors are estimated at each array on a sliding window by inverting the time delays between the sensors calculated with the cross-spectral method. A probabilistic approach is adopted whereby each measure and its error are represented by a probability density function (PDF). A weighted summation of the PDFs is carried out in which the stable directions of propagation are enhanced. The effects of the structural heterogeneities are taken into account by introducing an additional error associated to a robust hyperbolic secant (sech)-type PDF. The resulting PDFs of the back-azimuth are combined to calculate a PDF of the source location. The maximum likelihood of this PDF is taken as an estimate of the source position and its spread is characterized by a covariance analysis. Data from an experiment carried out at Arenal volcano (Costa Rica) with four arrays are analyzed. The precision and robustness of the method are tested by exploring the influence of the array configuration and other parameters. The mean standard deviation on the position of the sources is 600 m for the tremor and 400 m for the explosions and long-period (LP) events. Several tremors, explosions and LP events are analyzed and their sources located. The seismogenic zone is located in a 600 m radius area centered on the active crater. *INDEX TERMS:* 7280 Seismology: Volcano seismology (8419); 8419 Volcanology: Eruption monitoring (7280); 8494 Volcanology: Instruments and techniques; *KEYWORDS:* seismology, volcano, tremor, Arenal, array, slowness

Citation: Métaxian, J.-P., P. Lesage, and B. Valette, Locating sources of volcanic tremor and emergent events by seismic triangulation: Application to Arenal volcano, Costa Rica, *J. Geophys. Res.*, *107*(B10), 2243, doi:10.1029/2001JB000559, 2002.

1. Introduction

[2] Volcanic structures contain fluids, such as magma, water, vapor, gas, or diphasic mixtures of them, that fill cavities, such as magmatic chambers or conduits, dikes, cracks, or porous materials, embedded in solid rock. Fluid circulation, degassing, boiling or many other mechanisms can produce oscillations of the fluid-filled cavities which then radiate seismic waves called volcanic tremor or long-period (LP) events depending on their duration. These events are the most characteristic features of the seismic activity of volcanoes. Their study can provide important information on the physical processes which occur in volcanic systems. Tremor and LP events are characterized by sharp spectral peaks, related in many cases to resonance effects in fluid-filled cavities, by emergent onsets and by a lack of clear *S* waves. These features make the classical methods of hypocenter and focal mechanism determination by arrival time and polarization analysis inoperative. The deep tremor of Kilauea volcano is a particular case with sharp onsets which allows source location by using arrival times [*Aki and Koyanagi*, 1981]. However, in most volcanoes, the source positions of the LP events and tremor are difficult to retrieve although their determinations would be crucial for our understanding of volcanic systems and to improve eruption forecasting methods.

[3] Several alternative methods have been proposed for this purpose. Wave polarization has been used to estimate source location, either in two or three dimensions [*Del Pezzo et al.*, 1992; *Neuberg et al.*, 1994; *Chouet et al.*, 1999; *Legrand et al.*, 2000]. However, this procedure requires an a priori knowledge about the type of waves composing the wave field; moreover, free surface interactions [*Nuttli and Whitmore*, 1961; *Nuttli*, 1961], scattering and other propagation effects [*Hellweg*, 2000; *Neuberg and Pointer*, 2000] can strongly affect the spatial setting of the particle motion. Thus it seems difficult to obtain precise source positions from polarization analysis, with the exception of some specific cases. By inverting near-field waveforms of long-period signals (7.5 and 15 s) observed with about 10 broadband stations, *Legrand et al.* [2000] obtained

[1] Also at Institut de Recherche pour le Développement, Paris, France.
[2] Also at Coordination de la Recherche Volcanologique, Université Blaise Pascal, Aubière, France.

0148-0227/02/2001JB000559$09.00

both locations and focal mechanisms of long-period events and phreatic explosions at Aso volcano. The high accuracy of their method is partly attributed to the rapid spatial variations of the static displacement amplitudes observed in the near field.

[4] Methods based on cross correlation can be used when the distances between seismic sensors are not too large with respect to the dominant wavelengths of the signals. *Hurst* [1998] estimated the relative arrival times at several broadband stations by using a phase correlation method for bursts of tremor at Ruapehu volcano. He used a classical hypocenter determination routine to locate the source of the low-frequency events at depths ranging from 200 to 1000 m below the crater. *Yamaoka et al.* [1991] used a dense network of short-period seismographs to study the volcanic tremor at Izu-Oshima volcano. They calculated the phase delays between stations around 0.7 Hz by cross correlation and searched for the source location that minimized the residual between the observed and calculated delays. *Del Pezzo et al.* [1993] also used cross correlations to measure the phase shifts between stations of a small L-shaped array at Etna volcano. From these measurements, they estimated the direction and apparent velocity of propagation which are consistent with a source of tremor localized in the crater area. *Furumoto et al.* [1990] detected two separate sources of high-frequency tremor at Izu-Oshima volcano by applying the semblance technique [*Neidel and Tarner*, 1971] to records obtained with a dense array of short-period seismometers. By incorporating information contained in the rectilinearity of particle motions to the semblance method and by using a dense network of broadband stations, *Kawakatsu et al.* [2000] located the source of long-period tremor at depths of 1–1.5 km beneath the Izu-Oshima crater. The statistical correlation method of *Aki* [1957] yields the wave front orientation and thus the propagation direction of stochastic stationary wave fields. It also provides estimations of the phase velocities, which can be used to calculate velocity models of the structure. This method has been applied to seismo-volcanic events at Kilauea volcano [*Ferrazzini et al.*, 1991], Masaya caldera [*Métaxian et al.*, 1997] and Stromboli volcano [*Chouet et al.*, 1998]. *Métaxian et al.* [1997] also determined the direction of tremor wave propagation by the cross-spectral method and located the source by intersecting the directions estimated at several small arrays.

[5] Detailed studies of seismic wave fields, observed by small-aperture dense arrays, can be carried out with algorithms like the zero-lag cross-correlation method [*Frankel et al.*, 1991] or the Multiple Signal Classification, MUSIC [*Schmidt*, 1986; *Goldstein and Archuleta*, 1987]. They provide the back-azimuth and ray parameter of the main components of the wave field. Then the source location may be estimated by back-tracking rays down to a given epicentral distance. The zero-lag cross-correlation method has been used by *Del Pezzo et al.* [1997] at Teide volcano and by *Almendros et al.* [1997] and *Ibáñez et al.* [2000] at Deception Island. In order to take close sources into account and to locate them, *Almendros et al.* [1999] used this technique with the circular wave front approximation. *Saccorotti and Del Pezzo* [2000] made an analysis of uncertainties associated with the method using a probabilistic approach. *Goldstein and Chouet* [1994] evaluated the slowness spectra of volcanic tremor and gas piston events of Kilauea volcano and located their sources at depths shallower than 1 km beneath the Puu Oo crater. By using the same method and the wave polarization for the tremor and explosion quakes at Stromboli volcano, *Chouet et al.* [1997] estimated the source depths to be less than 200 m below the summit craters. They also showed how source and structural effects can explain the wave field complexity. *Saccorotti et al.* [1998] improved the results of *Chouet et al.* [1997] by performing a nonlinear Bayesian inversion of the slowness vector. Thus, the array analysis techniques have proved their ability to provide precise estimations of slowness vectors. In order to recover the source coordinates and depth, such estimations must be obtained simultaneously at several places. This was recently achieved by *La Rocca et al.* [2000] with two dense arrays deployed at Stromboli volcano and by *Almendros et al.* [2001a, 2001b] at Kilauea volcano with three seismic antennas. However, the deployment of several dense arrays, each composed of a great number of sensors, is not always feasible for logistic and economical reasons.

[6] In this paper, we address the problem of source location of volcanic tremor and emergent events by using a "light" method and a small number of seismic stations. Our objective is to design a low cost method which could be applied to volcano monitoring. Following a first experiment [*Métaxian et al.*, 1997], we propose to set up a network of small seismic antennas around the active zone of the volcano. Each antenna is the simplest possible dense array, i.e., a triangular array of vertical seismometers that can be connected by cable to a classical three-channel recorder or telemetry. At each antenna, the time delays between the sensors are measured using the cross-spectral method and the corresponding slowness vectors are estimated by inversion. We use a probabilistic approach to identify the significant values of back-azimuths and ray parameters and to determine the source position which best accounts for the whole array measurements. A description of the different steps of the procedure is presented and the method is validated by several tests of accuracy and robustness. The method is applied to the source location of the tremor, explosions, and LP events of Arenal volcano, Costa Rica.

2. Overview of the Method and Main Assumptions

[7] The proposed method of source location is based on some assumptions and is made up of several steps that are briefly described in this section. It is mainly aimed at locating sources of a volcanic tremor which is considered as a continuous stationary signal. At each array we have to extract information on the significant features of the wave field, such as the propagation direction and the apparent velocity. The first step of the procedure consists in measuring time delays between the seismometers of each array by using the cross-spectral method. Furthermore, the uncertainties on the time lags, which can be less than half the sampling spacing, are estimated and can thus be used in the subsequent steps of the procedure. These measurements are carried out on sliding time windows that move along the entire signals. In the second step, the apparent slowness vectors are estimated by inverting the time lags between all

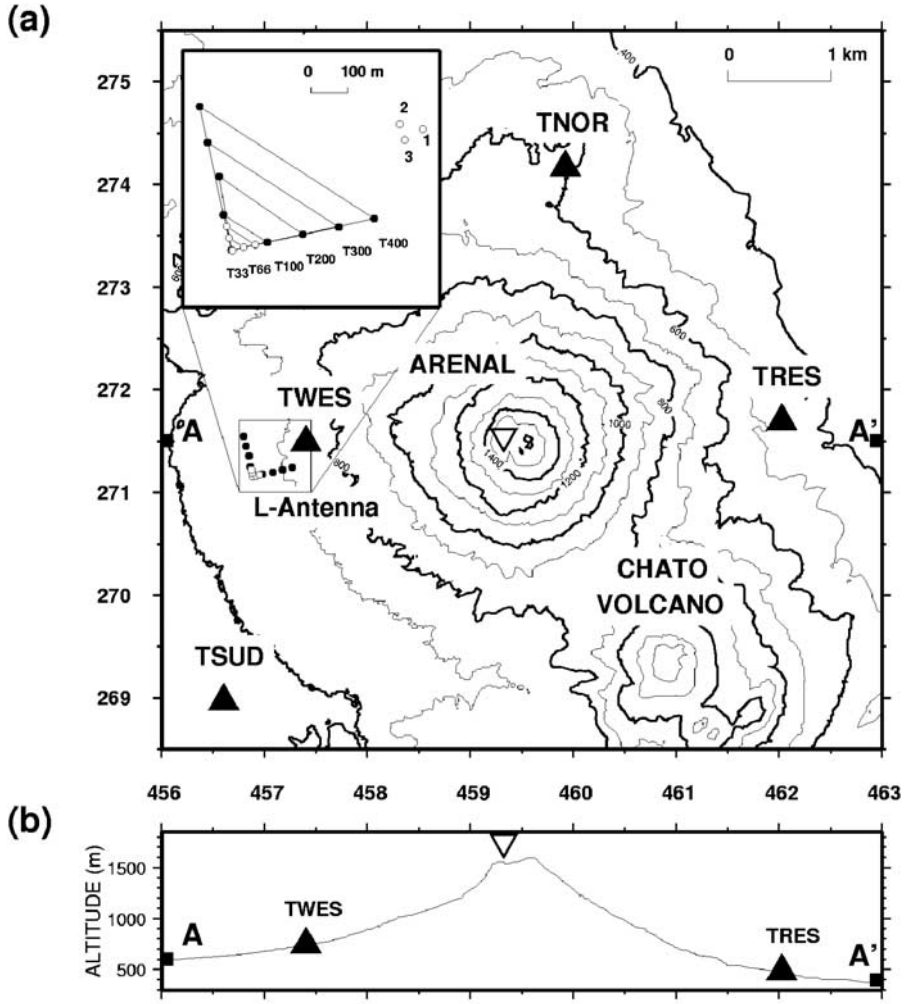

Figure 1. (a) Map of Arenal volcano showing the locations of the west active crater (open triangle), the triangular arrays (solid triangles), and the L-shaped array (circles). Inset is the configuration of the L-shaped and TWES antennas. Solid and open circles indicate the three-component L22 (2 Hz) and the vertical L4-C (1 Hz) seismometers, respectively. El Chato is an old inactive volcano located southeast of Arenal. The L-shaped and TWES antennas are situated on recent pyroclastic deposits dating from the actual eruptive cycle, while the other arrays lie on material from older eruptions. (b) Vertical cross section of the topography along line AA′ passing approximately through TWES, TRES, and the active crater. No vertical exaggeration.

pairs of sensors. These estimations are based on the following hypothesis: (1) the wave field is composed of plane waves and is nondispersive, (2) only one wave propagates across the array at the same time or, at least, one is dominant, and (3) the medium is laterally homogeneous underneath the array. Time series, either of slowness vectors or of back-azimuths and of apparent velocities, are obtained. They generally contain significant fluctuations. The next step consists in identifying, in the set of measures, the features of the waves propagating directly from the source and that can be used for the source location. We assume that the slowness values of direct waves are more stable and are obtained more frequently than those of waves resulting from scattering in the heterogeneous structure. A probabilistic approach is adopted in which each measure is represented by a probability density function (PDF). A weighted summation of the PDFs associated with all the measures is performed and a new PDF describing the wave parameters is obtained for each array. Strong or systematic errors in these parameters are taken into account by introducing an additional error associated with a robust probability distribution. In a final step, the source position is determined as the origin of the ray paths coming back from the different antennas. It is defined as the maximum likelihood of the probability density function describing the source position which is deduced from the slowness vector

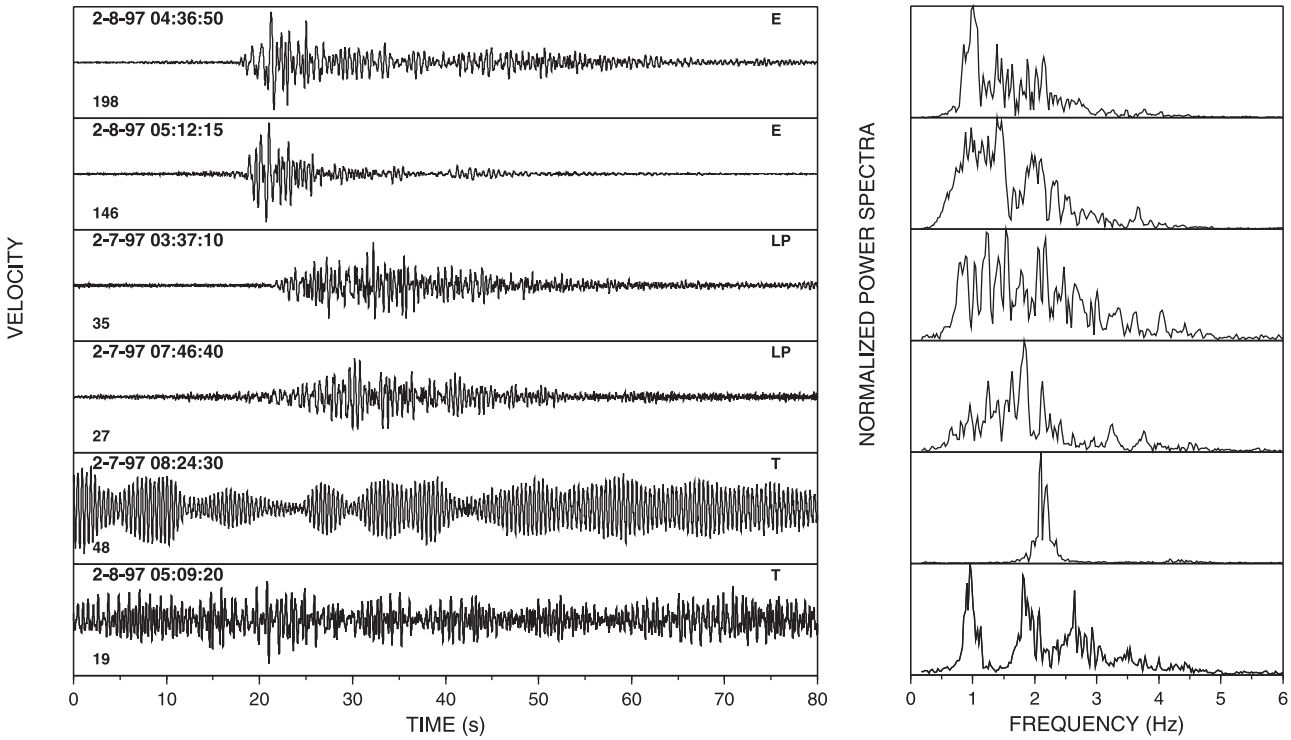

Figure 2. Velocity seismograms of typical explosions (E), long-period events (LP), and sections of tremor (T), recorded at antenna TWES (sensor 1), and corresponding normalized power spectra calculated on 40.96 s long windows. The date and time (UT) of the first sample and the maximum amplitude (μm s^{-1}) are indicated at the upper and lower left of the record, respectively.

PDFs of each array. The error on the source location is simply calculated from the PDF by a covariance analysis.

3. Seismic Arrays and Data

[8] A seismic experiment was carried out at Arenal volcano (Costa Rica) between 31 January and 10 February 1997 to study the sources of tremor and explosions, the wave field propagation and the surface velocity structure [*Mora et al.*, 2001]. Part of the experiment was designed to test and improve the method of seismic triangulation previously used at Masaya volcano [*Métaxian et al.*, 1997]. Arenal is a 1640 m above sea level (asl) high volcano located at the north of Costa Rica (10°28′N, 84°42′W). Since the large 1968 eruption, Arenal exhibited a permanent activity characterized by Strombolian explosions, gas emanations, lava flows, and sporadic pyroclastic flows [*Alvarado and Soto*, 2002]. Seismic activity includes a large variety of signals such as volcanic tremor, explosions, and long-period events [*Barquero et al.*, 1992].

[9] A network of four triangular arrays was set up around the volcano at distances between 2 and 3.8 km from the active crater (Figure 1). Each array was composed of three Mark Products L4-C vertical seismometers with a natural frequency of 1 Hz, connected by cable to a three-channel seismic recorder (LEAS-France, Sismalp-3 model) synchronized by a GPS receiver. The distance between sensors was about 60 m. The geometrical configuration of the antennas was surveyed by the geodetic service of the Instituto Costarricense de Electricidad with an electronic distance meter and a theodolite. The errors on the relative position of the seismometers are of the order of 1 cm. Simultaneous and continuous recordings with sampling frequency of 100 Hz were obtained at the four arrays from 4 to 10 February.

[10] A L-shaped array was deployed 2.5 km west of the summit with a radial branch oriented toward the crater (Figure 1, inset). It recorded 17 hours of seismic signal in continuous mode on 1 February 1997. Each branch was composed of two 1 Hz vertical L4-C seismometers located at 33 and 66 m from the vertex and four 2 Hz Mark Products L22 seismometers located at 100, 200, 300, and 400 m from the vertex. Two L4-C and one L22 seismometers were installed at the vertex. In section 7, the L-shaped array will be considered as a set of six triangular arrays with common vertex, each one being identified as triangle T_x, where x is the side length.

[11] During the experiment, the activity of Arenal was moderate with a daily average of 10 explosions occurring in the western crater, 30 long-period events and about 8 hours of tremor. Explosion quakes correspond to visually observed explosions. Unlike previous observations [*Métaxian et al.*, 1996; *Hagerty et al.*, 2000], the explosions were relatively weak and generally inaudible. No clear high-frequency acoustic phases are distinguishable in our 1997 records. Figure 2 shows typical seismograms of tremor, LP events and explosions recorded at TWES array and the corresponding normalized spectra. Tremor at Arenal can last from a few minutes to several hours. Tremor spectra display several regularly spaced peaks with relative amplitudes varying with time, the lowest frequency being near either 1 or 2 Hz. Amplitudes are clearly higher for explosions than for LP

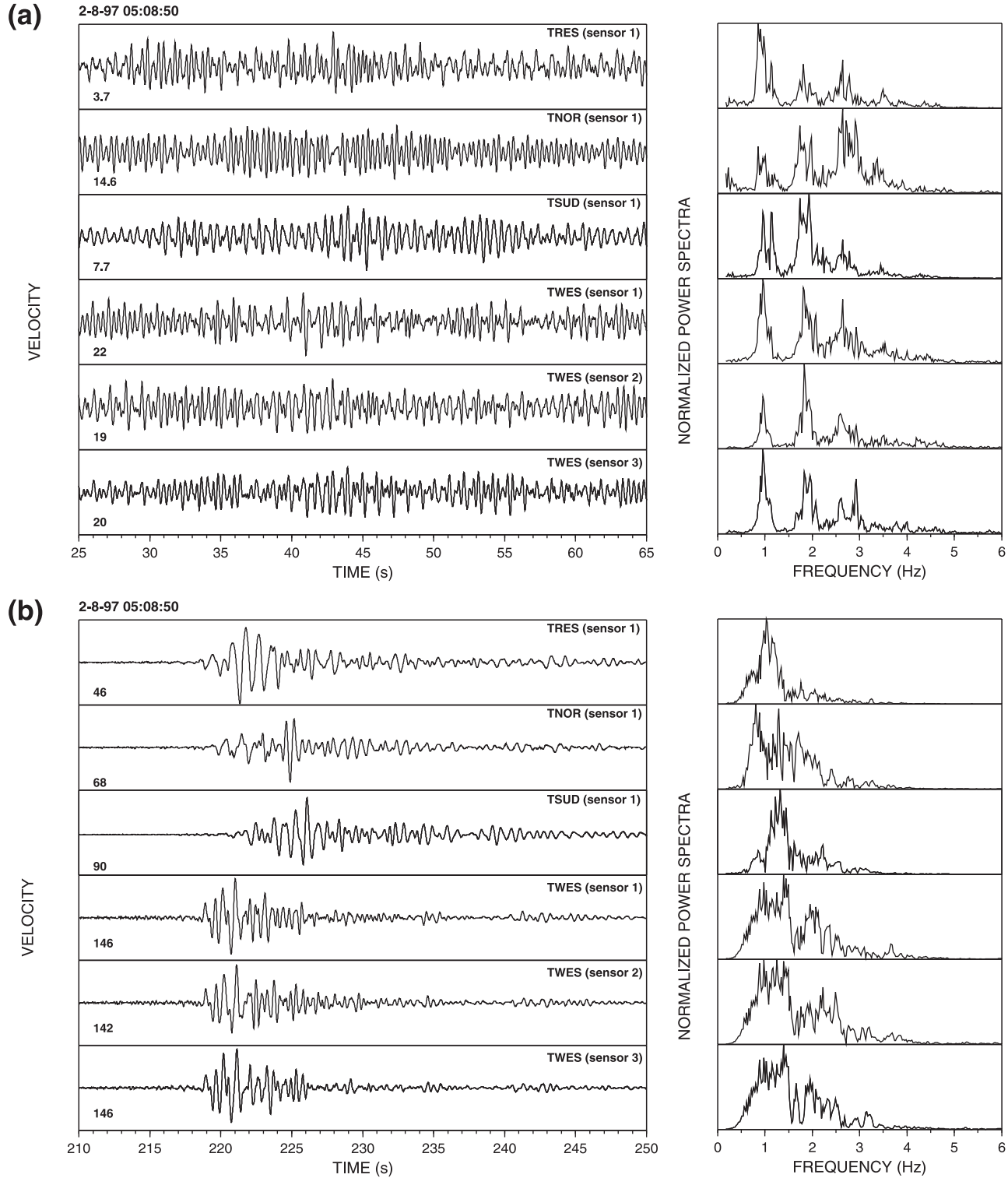

Figure 3. Velocity seismograms, and corresponding normalized spectra, of (a) a tremor and (b) an explosion. The records are obtained at sensor 1 of arrays TRES, TNOR, and TSUD and at the three sensors of TWES. Both signals are extracted from the record shown in Figure 5. The origin of the time axis is displayed at the upper left of the record. The maximum amplitudes, in μm/s, are given on the bottom left corner of the plots.

events. Nevertheless, the spectra of both types of events are similar with energy distributed in the range 0.5–5 Hz. Actually, there are probably no basic differences between explosions and LP events at Arenal, besides shallower sources, higher energy and, sometimes, acoustic phases for explosion quakes [*Métaxian et al.*, 1996; *Hagerty et al.*, 2000]. Figure 3 displays the seismograms and spectra of a section of tremor and of an explosion recorded at the four

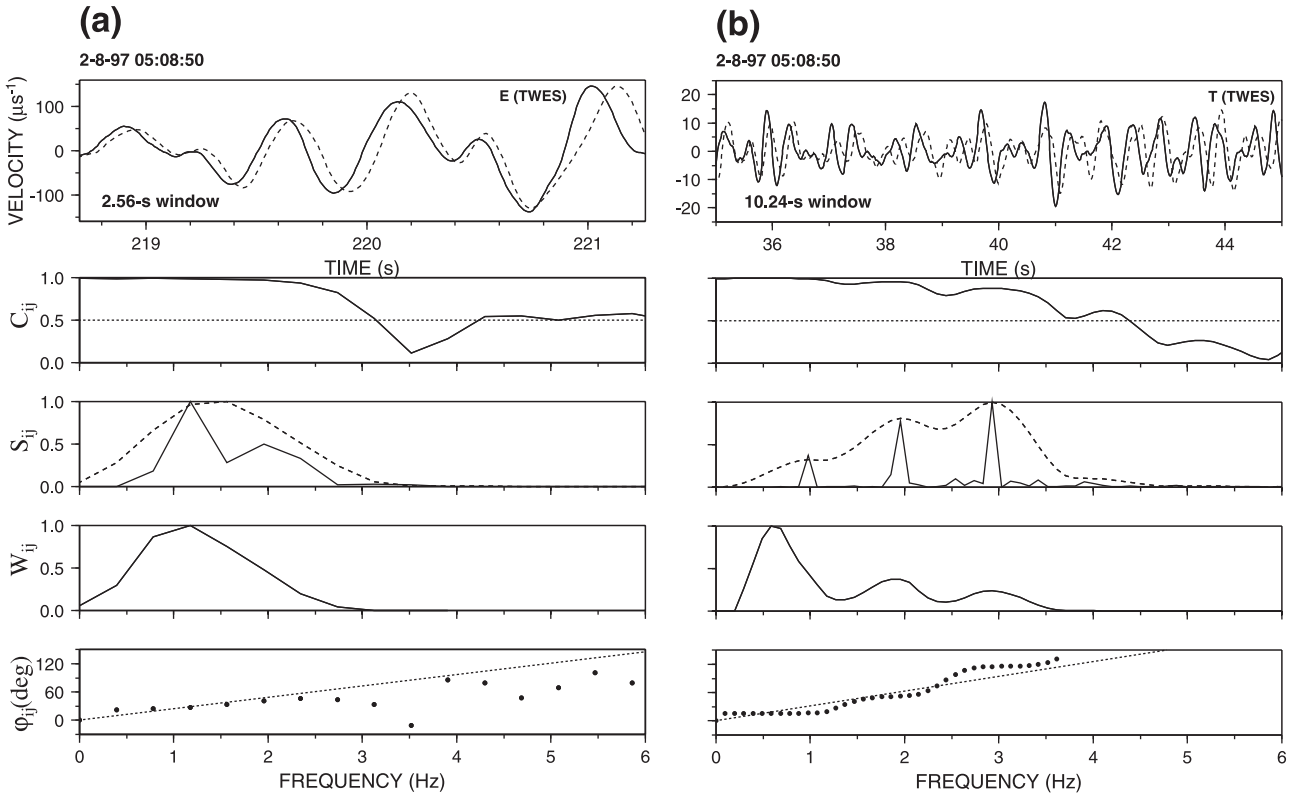

Figure 4. Examples of time delay calculation with the cross-spectral method. Two windows, including (a) the onset of an explosion and (b) a section of tremor, displayed in Figure 3, are analyzed. From top to bottom: the velocity seismograms obtained at sensors 1 (solid line) and 3 (dashed line) of array TWES; the coherency C_{ij} of the two signals; the normalized (solid line) and smoothed (dashed line) cross-spectra S_{ij}; the weight function W_{ij} used for the linear fit; the cross-spectrum phase φ_{ij} (dots) and the straight line obtained by weighted linear fit. The slope of the line is proportional to the time lag between the records.

triangular arrays. The spectra obtained at the different locations share common peaks which may be attributed to source effects. Nevertheless, differences in the relative amplitude of the peaks from one station to another indicate that path and site effects can strongly modify the wave amplitude at some frequencies, as shown by *Mora et al.* [2001]. The signals recorded by the three sensors of an array are generally characterized by a high degree of resemblance, especially at the beginning of the explosions (Figure 3).

4. Time Delay Measurement

[12] Time delays between each pair of seismometers ($N(N\text{-}1)/2$ pairs for N seismometers) are computed by using the cross-spectral method [*Jenkins and Watts*, 1968; *Poupinet et al.*, 1984; *Fréchet*, 1985] for successive time windows sliding along the seismograms. This method is based on the great similarity of the waveforms recorded by close sensors. Let $x_i(t)$ and $x_j(t) = \alpha\, x_i(t - \tau_{ij})$ be two seismic signals recorded by close seismometers i and j. The parameters $x_i(t)$ and $x_j(t)$ differ only by a scale factor α and a time delay τ_{ij} which can be expressed as a function of the cross-spectrum phase $\varphi_{ij}(f)$ by $\tau_{ij} = \varphi_{ij}(f)/2\pi f$, where f is the frequency. The similarity among pairs of signals is quantified through the coherency function which is defined as the smoothed cross-spectrum normalized by the product of the smoothed auto-spectra. A 1 Hz wide Hanning window is used for the smoothing. The time delay is obtained by a weighted linear fit of the cross-spectrum phase with the weight function defined as [*Fréchet*, 1985]:

$$W_{ij}(f) = \frac{|S_{ij}(f)|C_{ij}^2(f)}{1 - C_{ij}^2(f)}, \qquad (1)$$

where $C_{ij}(f)$ and $S_{ij}(f)$ are the coherency and the cross spectrum, respectively. The error on the delay is calculated from the variance in the estimate of the cross-spectrum phase. A first estimation of the time delay is used to align the signals. Then a residual time delay is calculated from the cross spectrum of the shifted signals. The resulting time lag is thus the sum of this residual delay and of the time shift. This procedure gives a precision on the time delay less than half the sampling interval. Figure 4 shows examples of delay computations, for an explosion and a tremor, and displays the functions involved in the calculation. For these signals, the coherency is higher than 0.8 for frequencies up to 2.5 or 3.5 Hz. The phase-frequency relation is almost linear in the spectral range where the weight function is not negligible.

[13] The time window length is an important parameter for the delay estimation. Indeed, it controls the temporal resolution of the results and the number of phase samples for the linear fit. This number must be great enough to obtain robust and significant values. It also depends on the spectral band for which the weight function $W_{ij}(f)$ is not negligible. Short ($\sim$1 s) time windows can be used for

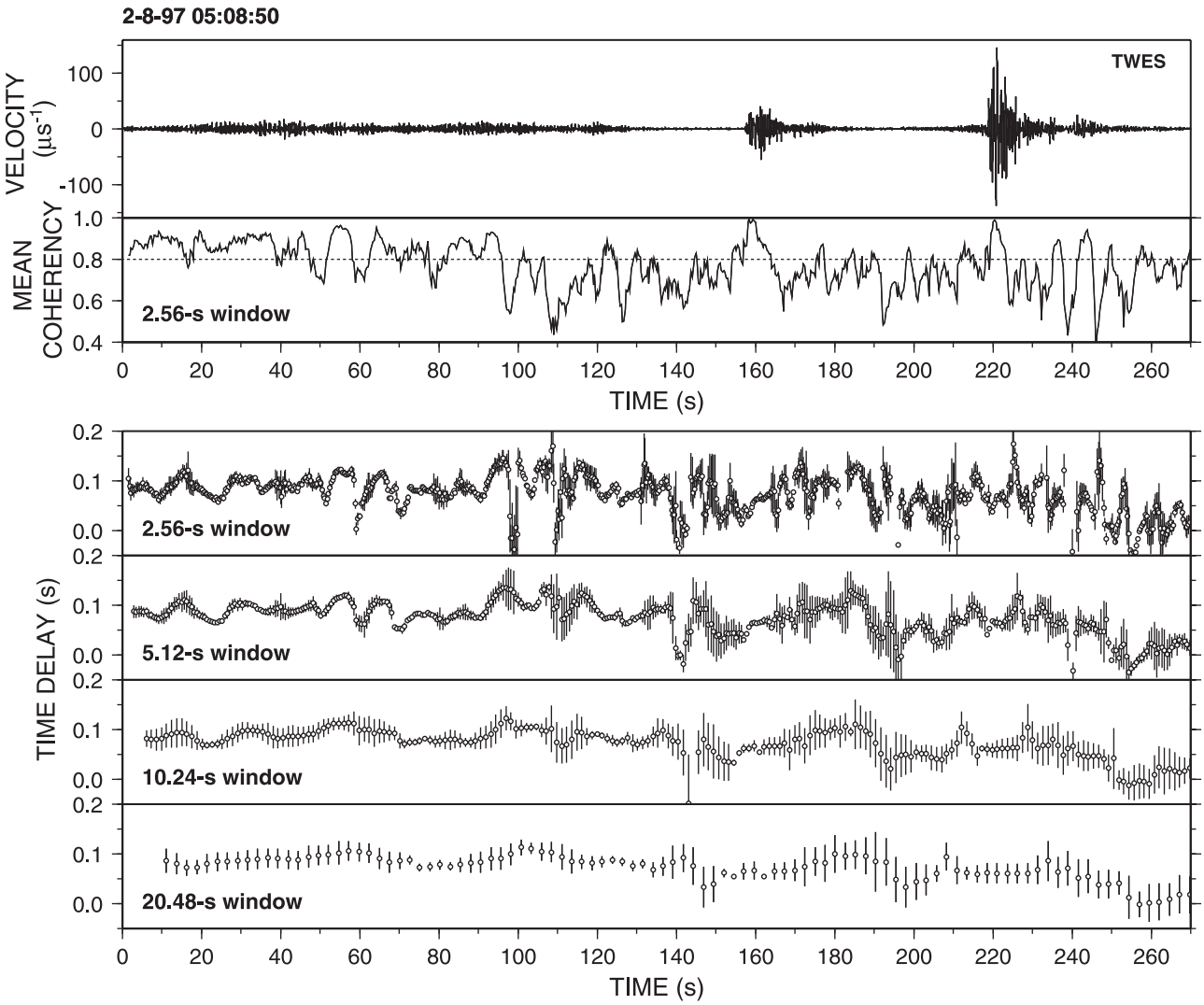

Figure 5. Influence of the analysis window length on the delay estimation. A 270 s long record obtained at TWES is taken as example. It includes the tremor and the explosion analyzed in Figures 3 and 4 as well as a LP event. The mean coherency for the three pairs of sensors, obtained with a 2.56 s sliding window, is displayed below the velocity seismogram. The delays between sensors 1 and 3 are calculated using four different window lengths (from top to bottom 2.56, 5.12, 10.24, and 20.48 s). The analysis window slides by steps of 12.5% of the window length. The delays and the corresponding error bars, estimated by the linear fit, are represented at the center time of each analysis window.

tectonic earthquakes because of their large (>10 Hz) bandwidth [*Got et al.*, 1994; *Got and Coutant*, 1997]. Conversely, since the spectral bands of LP events and tremor are narrower (<5 Hz), the time windows must be longer. To illustrate the influence of this parameter, Figure 5 displays the time delays obtained with four different window lengths ranging from 2.56 to 20.48 s. The mean coherency is defined as the average of the coherency values obtained in the frequency band of the signal and for the different pairs of sensors. The mean coherency is higher than 0.8 for the tremor and is close to 1 at the onset of the LP event and the explosion. Figure 5 illustrates also that the smoothing effect on the delays increases with increasing window lengths. We performed some numerical tests to determine an optimal window, taking this effect, the errors and robustness of the delay estimations and the computational efficiency into account. Optimal lengths of 10.24 s and 2.56 s were obtained respectively for the tremor and discrete events. Figure 6 shows the time delays between the sensors of TWES for the tremor and the explosion displayed in Figure 5. For both events, the delays are stable when the mean coherency is high. Conversely, when the coherency is low, as for example during the explosion coda, the time lags are characterized by a high variability and strong errors that made them unreliable.

5. Estimating the Slowness Vector

[14] The time delay between seismometers i and j can be written

$$\tau_{ij} = \mathbf{s} \cdot \mathbf{r}_{ij}, \tag{2}$$

where the dot denotes the usual scalar product, $\mathbf{s} = (-s \sin\theta, -s \cos\theta)$ is the slowness vector, θ is the back-azimuth,

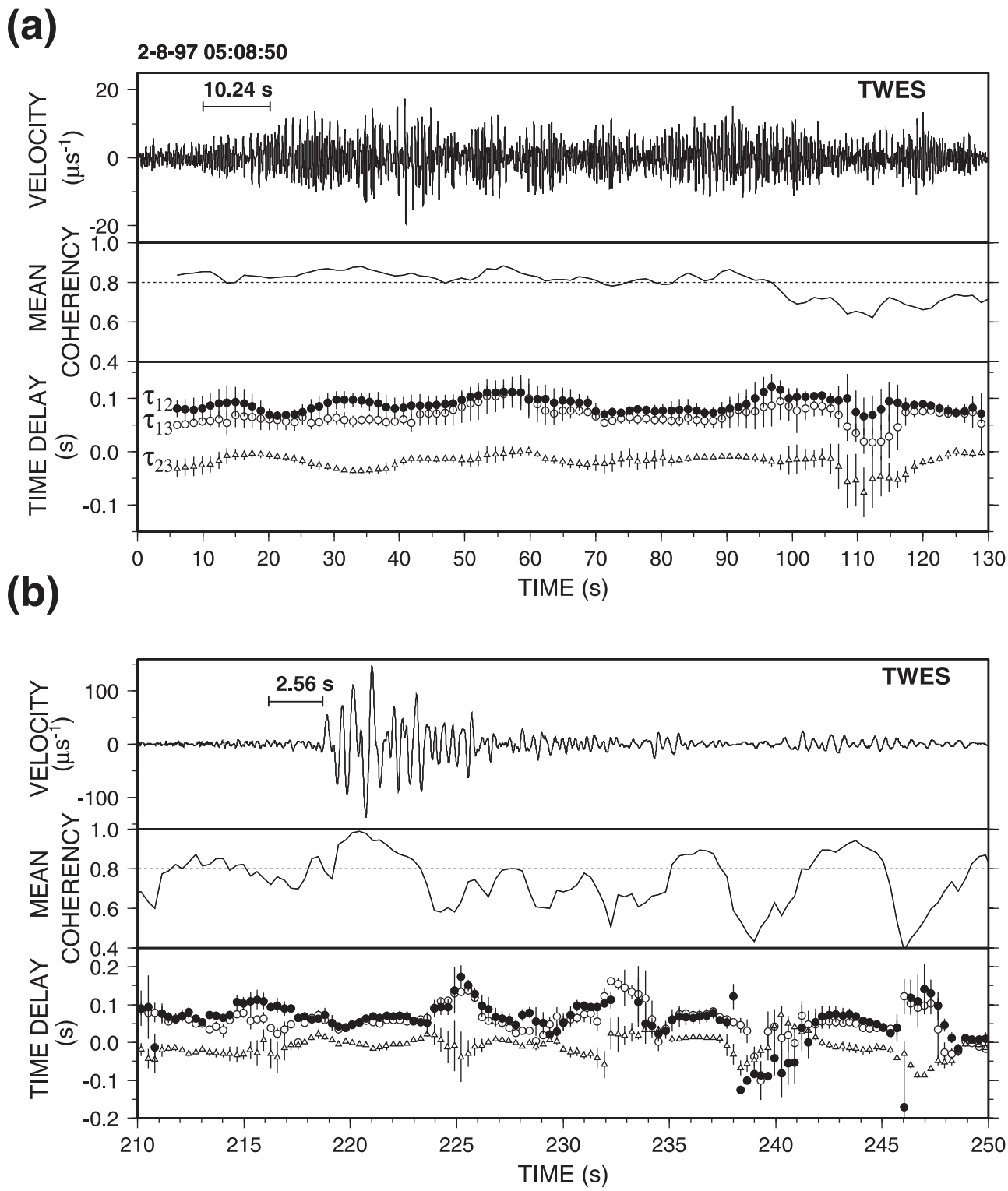

Figure 6. Velocity seismogram, mean coherency and time delays τ_{ij} between the three pairs of sensors of TWES, for (a) the tremor and (b) the explosion displayed in Figure 5. The analysis window length used for each signal is shown by a horizontal bar. The delays are generally stable, and the errors small, when the mean coherency is high.

measured clockwise from the north, $\mathbf{r}_{ij} = (r_{ij} \sin \phi_{ij}, r_{ij} \cos \phi_{ij})$ is the relative position vector, r_{ij} and ϕ_{ij} the corresponding distance and azimuth. Given a set of time delays τ_{ij}, and errors $\sigma_{\tau_{ij}}$, estimated for an antenna and a time window, the corresponding slowness vector **s** can be recovered by inversion. Depending on the assumptions, the inverse problem is either (1) linear or (2) nonlinear:

1. The vectors $\boldsymbol{r}_{ij}$ are assumed to be perfectly known and the theory underlying equation (2) is supposed to be perfectly right, i.e., the wave field includes a single plane

wave. The two components of the slowness vector are estimated by linear inversion of the $N(N\text{-}1)/2$ equations (2), where N is the number of sensors in the array. The problem is overdetermined for $N \geq 3$ and can be solved by standard least squares method.

2. Wave field complexity or local heterogeneities induce distortions of the wave front and thus errors on the theoretical relation (2). These errors can be taken into account by introducing errors on the array geometry. The vectors $\boldsymbol{r}_{ij}$ are now considered as parameters as well as $\mathbf{s}$. They are all estimated through a nonlinear inversion using equation (23) of *Tarantola and Valette* [1982a] and equation (44) for the calculation of the a posteriori covariance. As the array geometry is well determined, large differences between a posteriori and a priori positions can only be due to errors in the data or in the theory. Thus a posteriori distortion of the array geometry can be used as an indicator of the adequacy of the theory. The a priori model includes the measured array geometry and arbitrary values of the slowness (10^{-3} s m^{-1}) and of the back-azimuth (0°). In order to avoid artifacts due to the a priori model, the errors on the model are chosen sufficiently large (20 cm for the components of r_{ij} and 5×10^{-3} s m^{-1} for the components of $\mathbf{s}$). The results obtained with linear and nonlinear inversions are similar unless the coherency is very low. The a posteriori standard deviations on the slowness are slightly higher and probably more realistic for the nonlinear case and are hence used afterward.

6. Probability Density Function of Slowness Vector

[15] At this stage, time series of slowness vector have been obtained at each triangular array, yielding time series of back-azimuth and apparent velocity. These parameters contain temporal fluctuations related to sequences of waves with different slowness vectors. To describe the next steps of the procedure, we will focus on the back-azimuth although it can be applied identically to the apparent velocity. For each array k and each window centered at time t, the least squares inversion described in section 5 yields the back-azimuth α as a Gaussian variable with mean $\theta_k(t)$, standard deviation $\sigma_k(t)$ and probability density function (PDF):

$$\rho_1^k(\alpha, t) = \frac{1}{\sqrt{2\pi}\sigma_k(t)\mathrm{erf}\left(\frac{\pi}{\sqrt{2}\sigma_k(t)}\right)} \exp\left\{-\frac{[\alpha - \theta_k(t)]^2}{2\sigma_k^2(t)}\right\}. \quad (3)$$

The term erf $\left(\pi/\sqrt{2}\sigma_k(t)\right)$ in the probability law normalization comes from the fact that angles are defined modulus 2π. Following *Tarantola and Valette* [1982b], in order to take all the information available into account, we make a weighted summation of the PDFs $\rho_1^k(\alpha, t)$ obtained along the selected signal:

$$\rho_2^k(\alpha) \propto \int_0^{T\max} \rho_1^k(\alpha, t) w_k(t) dt. \quad (4)$$

The weights $w_k(t)$ are chosen in order to take the quality of the back-azimuth measure into account. They enhance the PDFs, the mean of which is stable with respect to time. They are expressed as a function of the time derivatives $\dot{\tau}_{ij}$ of the delays and are smoothed by a short boxcar $\Pi(t)$:

$$w_k(t) \propto \left(\sum_{i,j} \left|\dot{\tau}_{ij}(t)\right|\right)^{-1} * \Pi(t), \quad (5)$$

where the asterisk denotes the convolution operation. The PDF $\rho_2^k(\alpha)$ is related to the probability that the waves come from azimuth α at antenna k. The angle α would also define the direction of the source if the medium were laterally homogeneous. However, in a real heterogeneous medium, multipath propagation can occur yielding multimodal PDFs. Furthermore, lateral ray bending may induce a bias when identifying α as the source azimuth. We take these propagation effects into account by convolving ρ_2^k by another PDF of sech-type with zero mean. The sech PDF corresponds to the L^2 norm for small misfits and to the L^1 norm for large deviations [*Crase et al.*, 1990; B. Valette and P. Lesage, Inferring mean Earth mechanical models from normal modes, mass and inertia, 1, Theoretical developments, submitted to *Geophysical Journal International*, 2001]. The resulting PDF for the source azimuth at antenna k is thus

$$\rho_3^k(\alpha) \propto \rho_2^k(\alpha) * \frac{1}{\cos h\{\alpha/\sigma_0\}}, \quad (6)$$

where σ_0 controls the variability of the discrepancy between the back-azimuth and the source azimuth. Its value has been fixed to 3°.

[16] Figure 7 displays the time series of back-azimuth and apparent velocity estimated at the four arrays for the tremor and explosion analyzed in Figure 6. The corresponding PDFs $\rho_3^k(\alpha)$ are also plotted. Similar results are obtained for the whole set of analyzed data. For the explosion, only a small number of values, obtained for the time windows which include the onset of the event, are used to calculate the PDFs. The probability density functions generally present a single peak, the width of which is related to the variability of the results. The maxima of the back-azimuth PDFs are close to the respective crater directions for both events. In the case of tremor, the peak position of the apparent velocity PDF is in the range [0.4–0.9 km s^{-1}] for arrays TNOR, TWES, and TSUD and of about 1.5 km s^{-1} for TRES. The former values are consistent with surface wave velocities while the latter suggests a high content of body waves in the records at TRES. In the case of the explosion, the dominant apparent velocities are in the range [0.8–2 km s^{-1}]. Higher velocities are obtained for the explosion than for the tremor. This is clearly related to the different types of waves contained in the signals: either body waves at the onset of the explosions or dominant surface waves for tremor. The higher apparent velocities obtained at TRES compared to the other arrays, especially for the tremor, could be due to a propagation effect. Indeed, array TRES is located on the east flank of the volcano, while the sources are below the west part of the summit area (as will be shown in section 8). The seismic waves have thus to travel through the active structure to reach TRES (see cross section, Figure 1). This could result in a lower

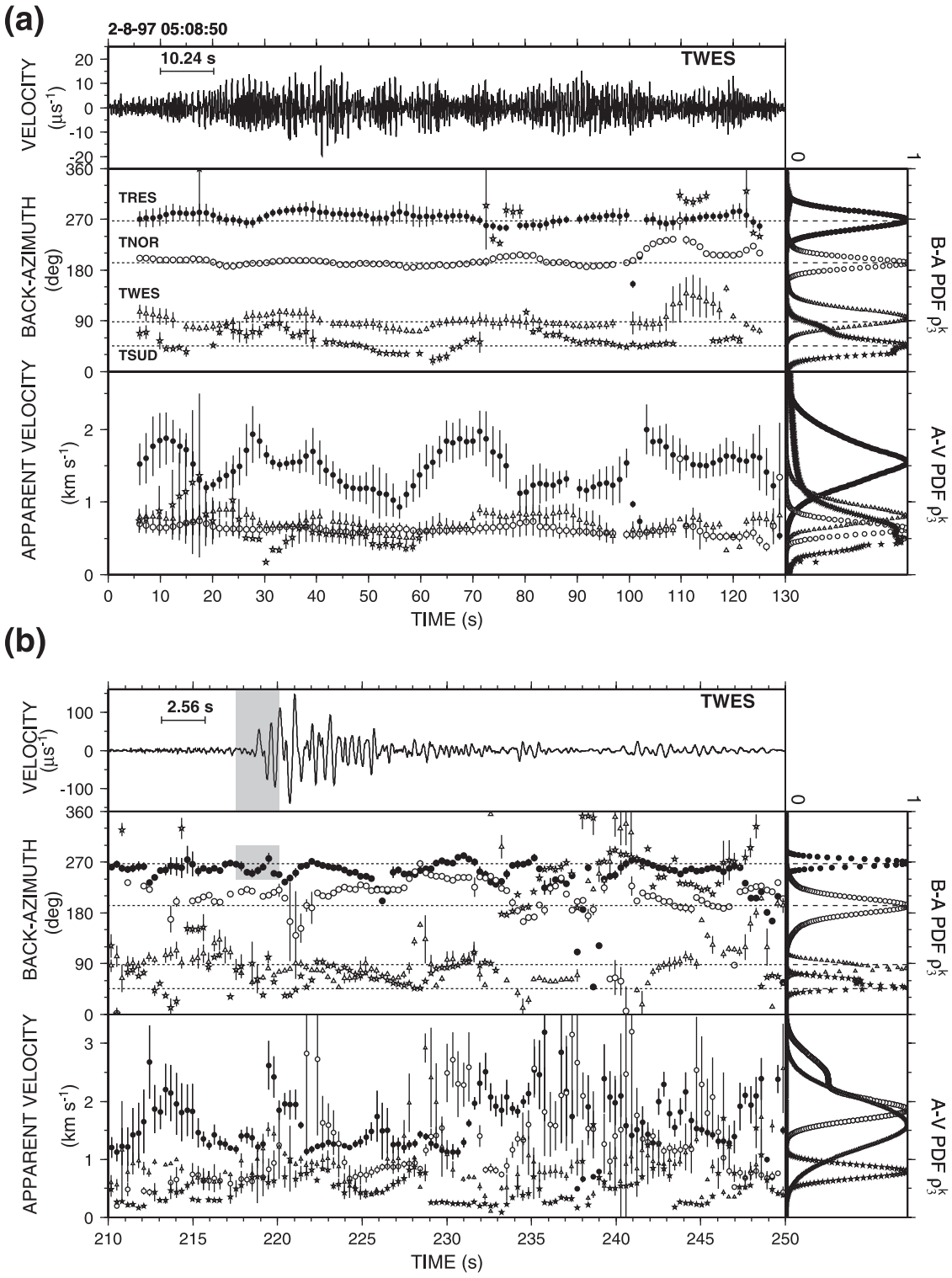

Figure 7. Back-azimuth, apparent velocity and associated errors versus time, estimated at the four triangular arrays for (a) the tremor and (b) the explosion of Figure 6. The window lengths used are indicated as horizontal bars above the seismograms. The time series are used to calculate the probability density function $\rho_3^k(\alpha)$ (equation (6)) of the back-azimuth (B-A) and apparent velocity (A-V) at each array. The crater direction is indicated by a dashed line for each antenna with the representations of the back-azimuths and their PDFs. In the case of the explosion, only the values obtained in a window centered on the first arrival are used to calculate the PDFs. This window is slightly different for each antenna because of the differences of arrival time. It is indicated by a gray shadow in the case of TWES.

amount of surface waves in the wave field and in higher incidence angles, and thus higher apparent velocities, for the body waves at the east side in comparison with the other parts of the structure.

7. Further Tests on Slowness Estimates

[17] The spatial resolution of an antenna is an increasing function of its width. On the other side, the coherency of two signals decreases, so the errors on delay measurements tend to increase, with increasing distances between the sensors. Thus an optimal distance between the components of the array has to be found. Furthermore, the estimation of the slowness vectors can be improved by adding more seismometers to the antenna, but this involves increasing costs. In this section, we consider the influence of the array characteristics on the slowness estimates. For this purpose, we compare the results produced by different subarrays of the L-shaped array (see inset in Figure 1): six tripartite antennas T_x, where x is the distance to the vertex, i.e., 33, 66, 100, 200, 300, and 400 m, two antennas of four sensors obtained by adding to T_{33} either the radial branch (L_{41}) or the transverse branch (L_{42}) seismometer of T_{66}, and one antenna of five sensors by merging T_{33} and T_{66}.

[18] Figure 8 displays the main results of the tests carried out with a tremor and an explosion. All the obtained back-azimuth PDFs have their maximum close to the crater direction (80°). The main differences are about the shape and width of the distributions which can be quantified by the corresponding standard deviation. The results obtained with T_{33} and T_{66} are very similar, with standard deviations of 15° and 20°, respectively for the tremor and 10° for the explosion. For array T_{100}, the standard deviations are 40° and 34° for the tremor and the explosion, respectively. They rapidly increase with distance for the larger arrays T_{200}, T_{300} and T_{400}. This is due to the low coherency between distant sensors, especially in the case of tremor. The antennas composed of four or five sensors produce slightly better results, with standard deviations of 11° and 8°, respectively, for the two events analyzed here. These results indicate that it is convenient to use antennas with distances between sensors less than 100 m in the frequency range 0.5–5 Hz. The use of more than three sensors slightly improves the slowness estimates.

8. Probability Density Function of the Source Position

[19] The last step of the procedure is to locate the source by using the information obtained at each antenna. For each point with geographical coordinates (x, y) in the source region and each array k, the back-azimuth $\alpha^k(x,y)$ and the corresponding value of ρ_3^k can be calculated. The measures produced by the different arrays are assumed to be independent. Therefore, the PDF of the source position is derived from the different PDF $\rho_3^k(\alpha^k)$ of back-azimuth as

$$\rho_4(x,y) \propto \prod_{k=1}^{N} \rho_3^k\left(\alpha^k(x,y)\right), \tag{7}$$

where N is the number of antennas. The maximum likelihood of the PDF ρ_4 yields an estimate of the source location. To measure the global coherency of the set of PDF ρ_3^k, following *Almendros et al.* [2001a], a criterion of location quality is useful to consider:

$$LQ = \frac{\max\left[\prod_{k=1}^{N} \rho_3^k\right]}{\prod_{k=1}^{N} \max\left(\rho_3^k\right)}, \qquad (0 < LQ \leq 1). \tag{8}$$

LQ is equal to one when all the maximum likelihood directions intersect at the same point. The precision of the source determination is related to the spread and shape of the PDF ρ_4. It can be characterized by both the mean quadratic radius $R = \sqrt{(\sigma_1^2 + \sigma_2^2)/2}$ and the aspect ratio $A_r = \sigma_2/\sigma_1$ ($\sigma_1 > \sigma_2$), where σ_1^2 and σ_2^2 are the principal variances of $\rho_4(x, y)$. The method could be extended to the estimation of the source depth if the following conditions were fulfilled: (1) the wave field is composed of body waves, (2) the apparent slowness is determined accurately at each antenna, and (3) the velocity structure is known, so the seismic rays can be retropropagated toward their origin.

[20] No velocity model was available for Arenal volcano. Only source locations in horizontal plane can thus be obtained. Figures 9a and 9b show the different back-azimuth PDFs $\rho_3^k(\alpha)$, represented as rose diagrams, and the probability density function of the source position $\rho_4(x, y)$ for the tremor and explosion already considered in Figure 7. In both cases, the maximum likelihood of ρ_4 (i.e., the estimation of the source position) is very close to the active crater. The quality of these estimations is attested by coefficients LQ equal to 0.93 and 0.62 and by radii R of 0.40 km and 0.34 km, for the tremor and the explosion, respectively. These examples illustrate the ability of the seismic triangulation method to give relatively precise estimates of the source position. The source location of the same events, obtained without using the sech PDF, is presented in Figures 9c and 9d. It is done by substituting ρ_3^k by ρ_2^k in equation (7). In this case the peak of the PDF ρ_4 is sharper, the quadratic mean radius R smaller (0.35 km and 0.25 km) and the maximum likelihood remains in the crater area. However, the corresponding location quality is lower (0.57 and 0.30), reflecting a greater difficulty in intersecting the propagation directions. Moreover, for the explosion, a secondary peak appears in ρ_4 at the northeast of the crater area. This shows that the use of sech probability functions results in more robust estimations. This is particularly important when processing low-quality data.

[21] We now evaluate the influence of the number and distribution of antennas on the source location by comparing the results obtained for the tremor with either four (Figure 9a), three (Figure 10a) or two (Figure 10b) antennas. The use of TSUD produces a poorly constrained position, unless when TWES and TNOR are included in the estimation. This is a consequence of the bimodal distribution of the corresponding PDF ρ_3^k, which probably results from strong scattered waves propagating through this array. The best results are obtained when TWES and TNOR are used together. Besides getting high quality measurements, these arrays constraint the source position in almost perpendicular directions. The inclusion of an additional antenna lowers the mean quadratic radius from 2 to 50% according to the case. The alignment of two antennas (e.g., TWES-TRES) with the source position results in redundant

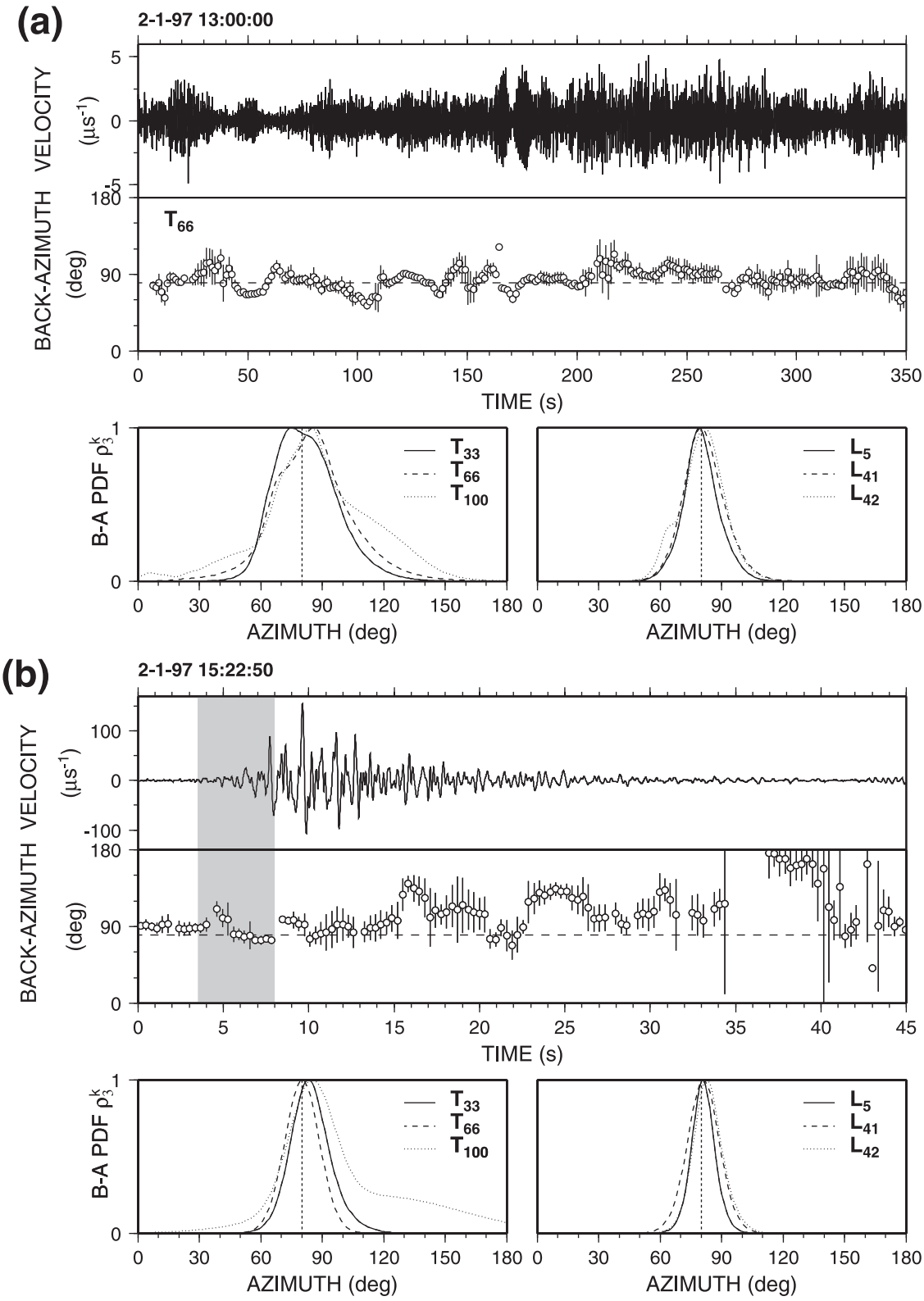

Figure 8. Influence of the antenna configuration on the back-azimuth estimates. For (a) a tremor and (b) an explosion, the back-azimuth PDFs ρ_3^k are calculated with different sub-arrays of the L-shaped array (see inset, Figure 1): three triangular arrays measuring 33, 66, or 100 m (T_{33}, T_{66}, and T_{100}), two arrays of four sensors (L_{41} and L_{42}) and one of five sensors (L_5). The crater azimuth is indicated by dashed lines. Also shown for reference are the time series of back-azimuth obtained with T_{66}. The date and origin time (UT) are indicated at the upper left of the records.

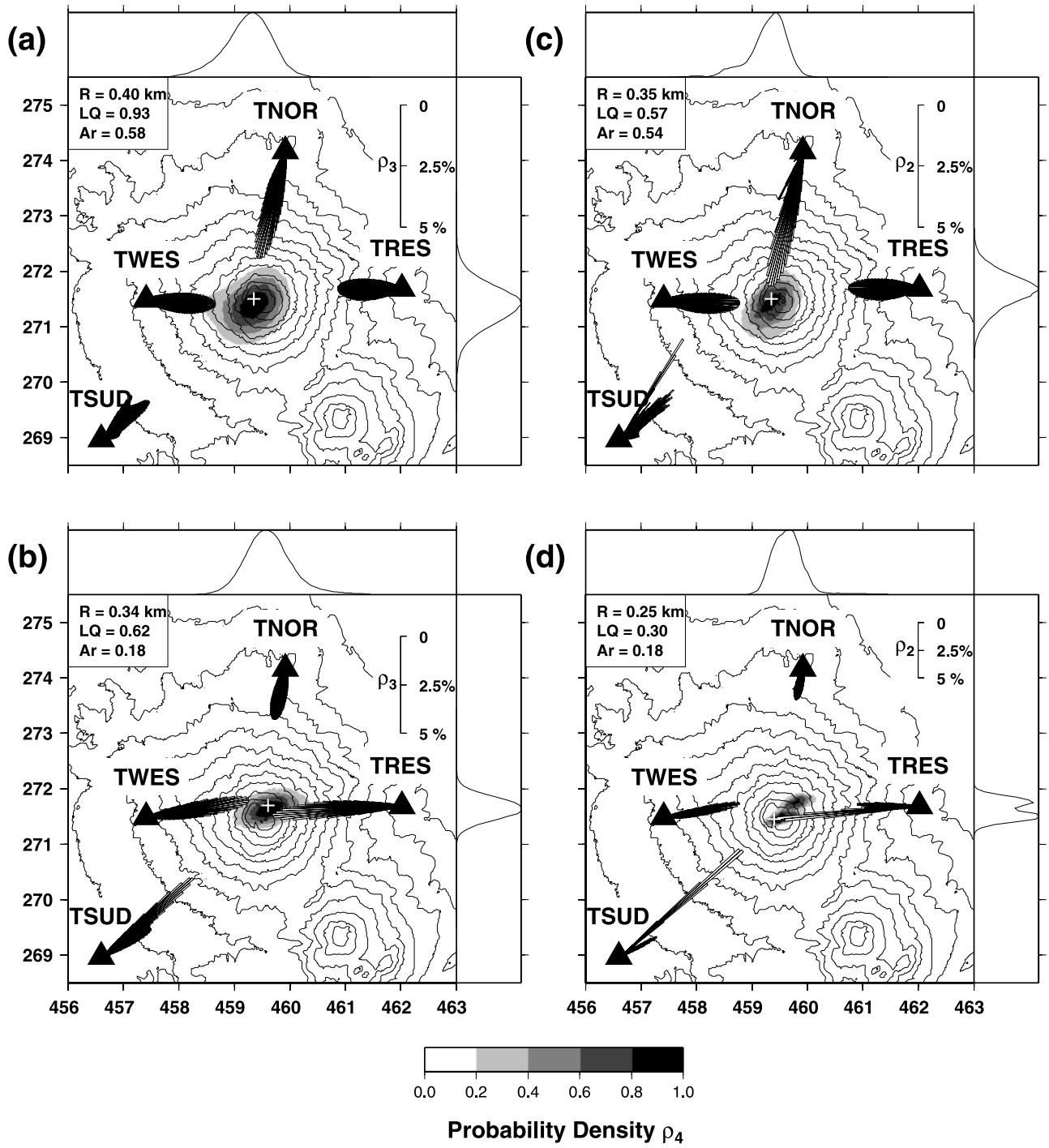

Figure 9. Probability density functions of the source position ρ_4 (equation (7)) for (a and c) the tremor and (b and d) the explosion displayed in Figures 6 and 7. For clarity, the PDFs ρ_4 are normalized by their maximum. On the right side and at the top of each map, the corresponding marginal laws $\int \rho_4(x, y)dx$ and $\int \rho_4(x, y)dy$ are plotted. The sech PDF, accounting for the heterogeneities of the medium, is used for the source locations in Figures 9a and 9b but not for Figures 9c and 9d. The PDFs ρ_2^k and ρ_3^k of the back-azimuth are represented as rose diagrams with 1° increments. The corresponding scale (in percent) is also plotted. Values of the mean quadratic radius (R), the location quality (LQ) and the aspect ratio (A_r) of the PDF ρ_4 are written on the upper left inset of each map. An open cross indicates the position of the maximum likelihood of ρ_4 which yields the source epicenter.

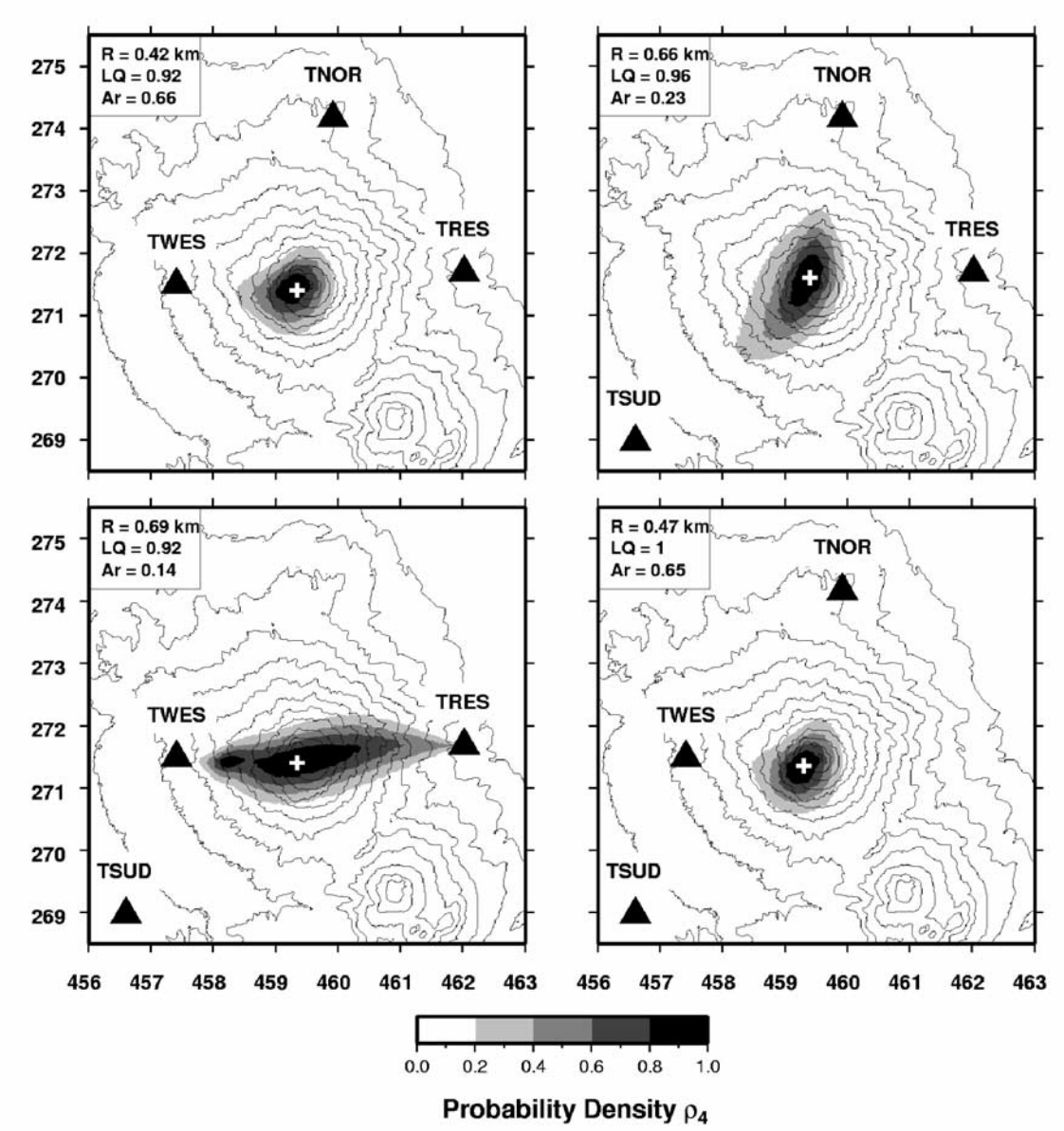

Figure 10. Probability density functions of the source position obtained with a reduced number of triangular antennas: (a) three antennas or (b) two antennas. The sech PDF is used in these locations. The tremor localized here is the same as in Figure 9a.

information on the back-azimuths. Note that *LQ* tends to increase when the number of antennas decreases as it becomes easier to intersect a lower number of directions. *LQ* is always equal to one when using two arrays and is no more a quality criterion in this case.

[22] Finally, a set of 45 records of tremor, with durations between 1 and 15 min, and a set including 25 explosions and 23 LP events, are selected. The sources of these events are localized by applying the procedure described above, using the four tripartite antennas and the sech PDF. Then the source position PDFs ρ_4^i of each set of events are averaged as

$$\rho_5(x,y) = \frac{1}{N_{\text{events}}} \sum_{i=1}^{N_{\text{events}}} \rho_4^i(x,y), \qquad (9)$$

where N_{events} is the number of events in the set. The PDF ρ_5 characterizes the active zone in the volcano. Both the distributions of the source locations and the functions ρ_5 show that the sources of seismic activity for both types of events are concentrated near the active crater (Figure 11). This analysis confirms that the seismogenic zones for the explosions and for the LP events almost completely overlap.

9. Discussion and Conclusion

[23] In order to locate seismo-volcanic sources, we propose an approach in which the slowness vectors are estimated using several elementary antennas, which act as seismic goniometers. A reasonably good precision on the source locations is permitted by using a great enough number of arrays. The deployment of many small antennas compensates the limited quality of the individual slowness measurements and the possible structural effects on the wave field.

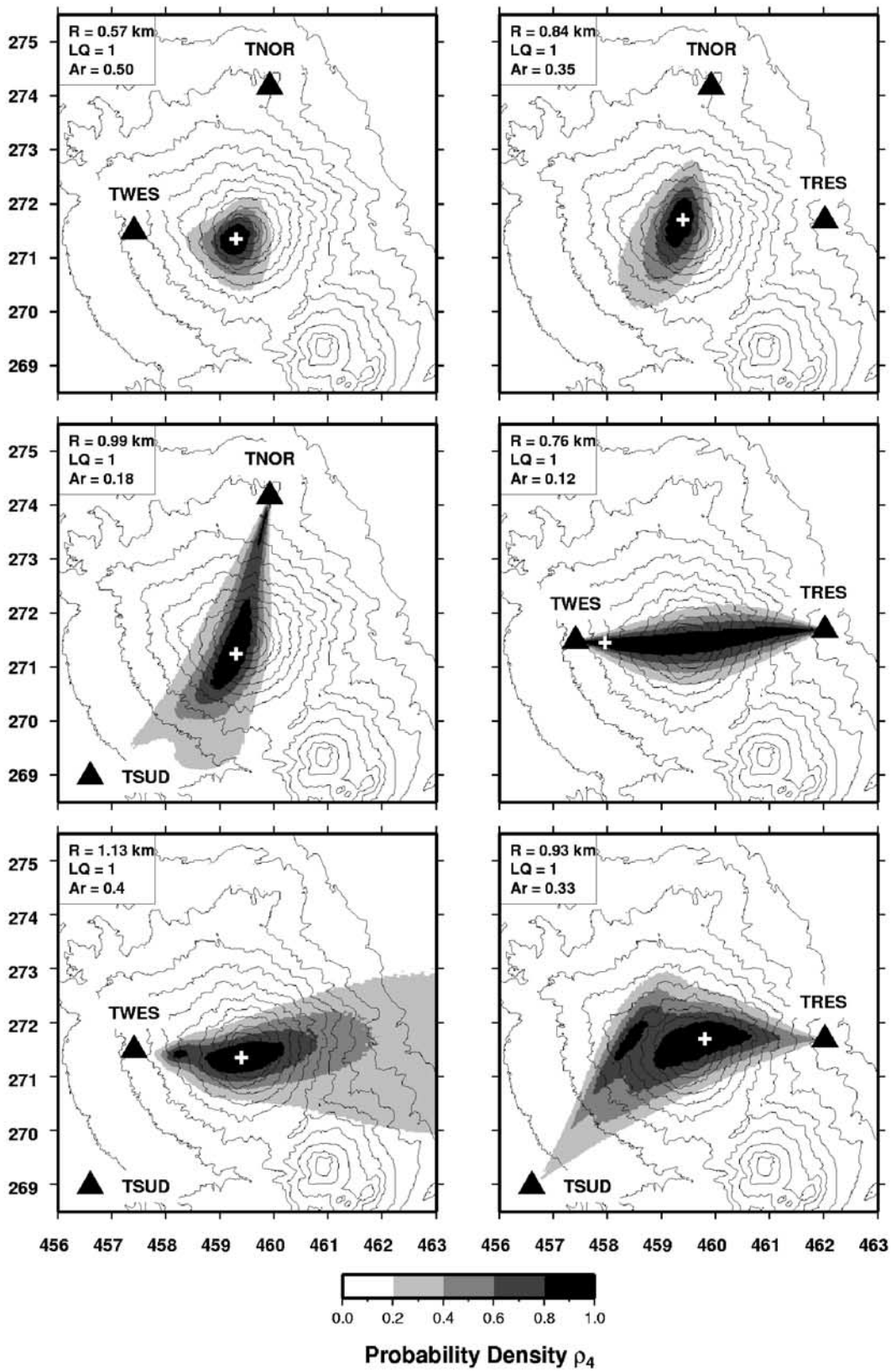

Figure 10. (continued)

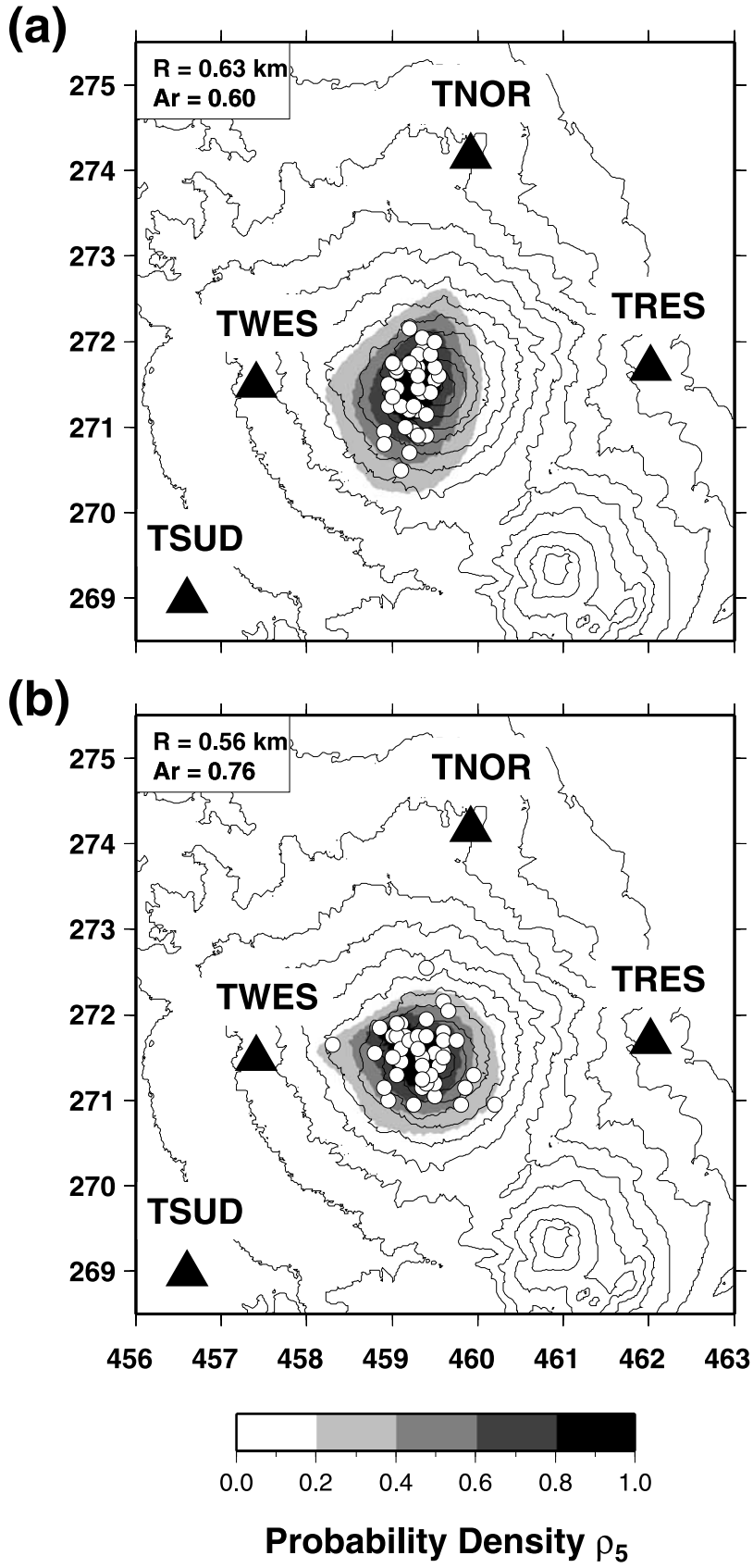

Figure 11. Stacked probability density functions ρ_5 (equation (9)) of the source location obtained with (a) 45 sections of tremor or (b) 25 explosions and 23 LP events. The normalized PDFs ρ_5 are shown in gray scale, and the corresponding mean quadratic radius and aspect ratio are indicated in the insets. The estimated source locations of each event are represented by open circles.

[24] The cross-spectral method adopted in this study yields high precision determinations of the time delays between the sensors. Moreover, it produces estimations of errors which are important components for the subsequent steps of the procedure. This method is well adapted to the analysis of tremor since it can retrieve the dominant features of the wave field with relatively long analysis windows. For highly nonstationary signals, as explosions, short time windows have to be used in order to analyze separately the successive wave trains. In this case, the cross-spectral method may be slightly less robust than the cross-correlation method. Nevertheless, the choice of the delay measurement method is probably not critical and both methods would produce similar results. The estimation of the slowness vector from the time delays is based on the assumption that only one nondispersive plane wave is propagating in a laterally homogeneous medium beneath the array. To process in detail complex wave fields including several plane waves, dense array analysis methods such as the MUSIC algorithm [*Goldstein and Archuleta*, 1987] must be used. This is not possible with triangular antennas. Nevertheless, our experiments show that reasonably good measurements of slowness vectors can be obtained with small arrays composed of only three vertical seismometers. Moreover, the robustness of the probabilistic approach used in the present can take the departure from the underlying assumptions into account. On the other hand, when the distance to the source is not much larger than the antenna width, the plane wave approximation is no longer justified. Equation (2) can be modified to take into account the circular wave front geometry by adding the epicentral distance to the parameters of the inverse problem [*Almendros et al.*, 1999].

[25] Because of the complex nature of the seismic wave field in volcanoes, the direction and apparent velocity of propagation at a given point are not constant over time. This leads to select the values which contain information on the source position. These values are supposed to be more probable and more stable over time. A key element of the method is thus to make weighted averages of the probability density functions representing the measures. The weight function enhances the features corresponding to stable sections of the records. This is specially useful for the processing of continuous signals as tremor. The resulting mean PDFs of back-azimuth generally display one sharp peak indicating that good measurements of the direction of propagation are achieved. The mean PDFs corresponding to the apparent velocity are wider than those of the azimuth. This reflects the nature of the wave field composed of a mixture of surface waves and body waves with varying incidence angles. In the case of LP events or explosions, the very beginning of the records is mainly composed of body waves. The corresponding slowness measurements can thus be used to estimate the source depth if the velocity structure is known [*Chouet et al.*, 1997; *Saccorotti et al.*, 1998; *Almendros et al.*, 2001a]. Unfortunately, no velocity model of Arenal volcano is available at the present time, precluding a depth estimation of the hypocenters in this study. The slowness vector estimations can be biased by lateral heterogeneities and topographic effects. Therefore the probability of a large difference between the estimated back-azimuth and the source direction is relatively high and not Gaussian. The convolution of the PDF ρ_2^k with the sech probability function, in addition to giving smoother distributions, produces more robust estimations of the source positions by allowing stronger deflections of the measured values. When introducing the sech PDF, the source position PDF $\rho_4(x, y)$ has a slightly larger mean radius than without the sech function. However, the location quality LQ is higher indicating that the back-azimuth PDFs obtained at the different antennas are more internally consistent.

[26] The number of antennas is one of the most critical elements for the resulting precision. It appears that a minimum of three arrays is necessary to ensure reliable source locations. The use of more arrays can reinforce the robustness of the method and increase the precision. Moreover, it is possible to set up all the arrays in a 180° sector of the volcano from the active zone without lowering the precision. The results obtained with array TSUD provide a good illustration of the effects of poor quality measurements. The apparent velocities estimated at TSUD are systematically the lowest among the four antennas. It could result from a local site effect since the antenna is located on a relatively flat area with very low consolidated material at the surface. On the other hand, most of the back-azimuth PDFs obtained at TSUD display a bimodal distribution which could reflect multipathing or strongly scattered waves at this site. This distribution produces a significant decrease of the location quality when only three antennas, including TSUD, are used. With four arrays, the influence of TSUD is much lower. In the latter case, the mean errors on the source position are 580 and 440 m for the tremor and the explosions respectively. They are greater than those obtained at Kilauea volcano (200 m) by *Almendros et al.* [2001b] using very dense arrays and high precision structural model. Nevertheless the precision obtained with triangular arrays is sufficient to determine the active seismic zones in a volcano. At Arenal volcano, the epicenters estimated for the tremors, explosions and LP events are all concentrated in a small area centered on the active crater. The mean radii of the stacked PDF of position are 630 m and 560 m respectively for the tremor and for the explosions and LP events. The corresponding maxima of probability are located on the crater, retrieving the expected position of the sources.

[27] By using average first arrival times, *Hagerty et al.* [2000] located the sources of Arenal explosions a few hundreds of meters southeast from the summit. This illustrates the difficulties in locating sources from arrival times of emergent onsets. On the other side, our results indicate that it is possible to determine the source position in the horizontal plane of both emergent events and volcanic tremor with a network of small antennas. The next stage of this study would be to obtain velocity models of the Arenal structure. Indeed, it will be important to extend the method to the estimation of source depths and to compare the results obtained for the different types of event. Furthermore, the procedure described in this paper requires a limited amount of seismic equipment and computing time. It can be adapted thus to real-time volcano monitoring.

[28] **Acknowledgments.** We thank the entire staff of the Area de Amenazas y Auscultacíon Sismovolcánica of the Instituto Costarricense de Electricidad (ICE), especially Guillermo Alvarado and Rafael Barquero, Mauricio Mora (University of Costa Rica) and Jacques Dorel (Observatoire

de Physique du Globe de Clermont-Ferrand) for their participation in the field work. The geodetic team of ICE is acknowledged for surveying the seismic arrays. We are indebted to David Marsan for careful readings of the manuscript. We are grateful to Alan Linde, Gaetano De Luca, and an anonymous reviewer for constructive comments. This work was supported by the Programme Régional pour la Prévention du Risque Volcanique en Amérique Centrale (PREVO-MAE), the Programme National de Recherche sur la Prévision et la Prévention des Risques Naturels (PNRN-INSU), the Coordination de la Recherche Volcanologique (CRV-CNRS), the Institut de Recherche pour le Développement and the Université de Savoie.

References

Aki, K., Space and time spectra of stationary stochastic waves, with special reference to microtremors, *Bull Earthquake Res. Inst. Univ. Tokyo*, *25*, 415–457, 1957.

Aki, K., and R. Koyanagi, Deep volcanic tremor and magma ascent mechanism under Kilauea Hawaii, *J. Geophys. Res.*, *86*, 7095–7109, 1981.

Almendros, J., J. Ibáñez, G. Alguacil, E. Del Pezzo, and R. Ortiz, Array tracking of the volcanic tremor source at Deception Island, Antartica, *Geophys. Res. Lett.*, *24*, 3069–3072, 1997.

Almendros, J., J. Ibáñez, G. Alguacil, and E. Del Pezzo, Array analysis using circular wave-front geometry: An application to locate the nearby seismo-volcanic source, *Geophys. J. Int.*, *136*, 159–170, 1999.

Almendros, J., B. Chouet, and P. Dawson, Spatial extent of a hydrothermal system at Kilauea volcano, Hawaii, determined from array analyses of shallow long-period seismicity, 1, Method, *J. Geophys. Res.*, *106*, 13,565–13,580, 2001a.

Almendros, J., B. Chouet, and P. Dawson, Spatial extent of a hydrothermal system at Kilauea volcano, Hawaii, determined from array analyses of shallow long-period seismicity, 2, Results, *J. Geophys. Res.*, *106*, 13,581–13,597, 2001b.

Alvarado, G. E., and G. J. Soto, Pyroclastic flow generated by crater-wall collapse and outpouring of the lava pool of Arenal volcano, Costa Rica, *Bull. Volcanol.*, *63*, 557–568, 2002.

Barquero, R., G. E. Alvarado, and T. Matumoto, Arenal volcano (Costa Rica) premonitory seismicity, in *Volcanic Seismology*, edited by P. Gasparini, R. Scarpa, and K. Aki, pp. 84–96, Springer-Verlag, New York, 1992.

Chouet, B., G. Saccorotti, M. Martini, P. Dawson, G. De Luca, G. Milana, and R. Scarpa, Source and path effects in the wave fields of tremor and explosions at Stromboli volcano, Italy, *J. Geophys. Res.*, *102*, 15,129–15,150, 1997.

Chouet, B., G. De Luca, G. Milana, P. Dawson, M. Martini, and R. Scarpa, Shallow velocity structure of Stromboli volcano, Italy, derived from small-aperture array measurements of strombolian tremor, *Bull. Seismol. Soc. Am.*, *88*, 653–666, 1998.

Chouet, B. A., G. Saccoroti, P. Dawson, M. Martini, R. Scarpa, G. De Luca, G. Milana, and M. Cattaneo, Broadband measurements of the sources of explosions at Stromboli volcano, Italy, *Geophys. Res. Lett.*, *26*, 1937–1940, 1999.

Crase, E., A. Pica, M. Noble, J. McDonald, and A. Tarantola, Robust elastic nonlinear waveform inversion: Application to real data, *Geophysics*, *55*, 527–538, 1990.

Del Pezzo, F., C. Godano, A. Gorini, and M. Martini, Wave polarization and location of the source of the explosion quakes at Stromboli volcano, in *Volcanic Seismology*, edited by P. Gasparini, R. Scarpa, and K. Aki, pp. 279–296, Springer-Verlag, New York, 1992.

Del Pezzo, E., S. De Martino, S. Gresta, M. Martini, G. Milana, D. Patané, and C. Sabbarese, Velocity and spectral characteristics of the volcanic tremor at Etna deduced by a small seismometer array, *J. Volcanol. Geotherm. Res.*, *56*, 369–378, 1993.

Del Pezzo, E., M. La Rocca, and J. Ibáñez, Observations of high-frequency scattered waves using dense arrays at Teide volcano, *Bull. Seismol. Soc. Am.*, *87*, 1637–1647, 1997.

Ferrazzini, V., K. Aki, and B. Chouet, Characteristics of seismic waves composing Hawaiian volcanic tremor and gas-piston events observed by a near-source array, *J. Geophys. Res.*, *96*, 6199–6209, 1991.

Frankel, A., S. Hough, P. Friberg, and R. Busby, Observations of Loma Prieta aftershocks from a dense array in Sunnyvale, California, *Bull. Seismol. Soc. Am.*, *80*, 1900–1922, 1991.

Fréchet, J., Sismogénèse et doublets sismiques, thèse d'état, 207 pp., Univ. Sci. Technol. Médec., Grenoble, France, 1985.

Furumoto, M., T. Kunitomo, H. Inoue, I. Yamada, K. Yamaoka, A. Ikami, and Y. Fukao, Twin sources of high-frequency volcanic tremor of Izu-Oshima volcano, Japan, *Geophys. Res. Lett.*, *17*, 25–27, 1990.

Goldstein, P., and R. J. Archuleta, Array analysis of seismic signals, *Geophys. Res. Lett.*, *14*, 13–16, 1987.

Goldstein, P., and B. Chouet, Array measurements and modeling of sources of shallow volcanic tremor at Kilauea volcano, Hawaii, *J. Geophys. Res.*, *99*, 2637–2652, 1994.

Got, J.-L., and O. Coutant, Anisotropic scattering and travel time delay analysis in Kilauea volcano, Hawaii, earthquake coda waves, *J. Geophys. Res.*, *102*, 8397–8410, 1997.

Got, J.-L., J. Fréchet, and F. W. Klein, Deep fault plane geometry inferred from multiplet relative relocation beneath the south flank of Kilauea, *J. Geophys. Res.*, *99*, 15,375–15,386, 1994.

Hagerty, M. T., S. Y. Schwartz, M. A. Garcés, and M. Protti, Analysis of seismic and acoustic observations at Arenal Volcan, Costa Rica, 1995–1997, *J. Volcanol. Geotherm. Res.*, *101*, 27–65, 2000.

Hellweg, M., Volcanic tremor and physical source models: Lascar volcano, Chile. Ph.D. thesis, Inst. für Geophys. der Univ. Stuttgart, 2000.

Hurst, A. W., Shallow seismicity beneath Ruapehu crater lake: Results of a 1994 seismometer deployment, *Bull. Volcanol.*, *60*, 1–9, 1998.

Ibáñez, J. M., E. Del Pezzo, J. Almendros, M. La Rocca, G. Alguacil, R. Ortiz, and A. García, Seismovolcanic signals at Deception Island volcano, Antarctica: Wave field analysis and source modeling, *J. Geophys. Res.*, *105*, 13,905–13,931, 2000.

Jenkins, G. M., and D. G. Watts, *Spectral Analysis and Its Applications*, Holden-Day, Boca Raton, Fla., 1968.

Kawakatsu, H., S. Kaneshima, H. Matsubayashi, T. Ohminato, Y. Sudo, T. Tsuitsui, K. Uhira, H. Yamasato, H. Ito, and D. Legrand, Aso94: Aso seismic observation with broadband instruments, *J. Volcanol. Geotherm. Res.*, *101*, 129–154, 2000.

La Rocca, M., S. Petrosino, G. Saccorotti, M. Simini, J. Ibáñez, J. Almendros, and E. Del Pezzo, Location of the source and shallow velocity model deduced from the explosion quakes recorded by two antennas at Stromboli volcano, *Phys. Chem. Earth*, *25*, 731–735, 2000.

Legrand, D., S. Kaneshima, and H. Kawakatsu, Moment tensor analysis of near-field broadband waveforms observed at Aso, Japan, *J. Volcanol. Geotherm. Res.*, *101*, 155–169, 2000.

Métaxian, J. P., P. Lesage, R. Barquero, and A. Creusot-Eon, Caracteristicas expectrales de las señales sísmicas y estimación de V_p en la estructura superficial del Volcán Arenal, *Bol. Obs. Vulcanol. Arenal*, *6*(11–12), 23–44, 1996.

Métaxian, J. P., P. Lesage, and J. Dorel, Permanent tremor of Masaya volcano, Nicaragua: Wave field analysis and source location, *J. Geophys. Res.*, *102*, 22,529–22,545, 1997.

Mora, M. M., P. Lesage, J. Dorel, P.-Y. Bard, J. P. Métaxian, G. E. Alvarado, and C. Leandro, Detection of seismic site effects by using H/V spectral ratios at Arenal volcano (Cost Rica), *Geophys. Res. Lett.*, *28*, 2991–2994, 2001.

Neidel, N. S., and T. M. Tarner, Semblance and other coherency measure for multichannel data, *Geophysics*, *36*, 482–497, 1971.

Neuberg, J., and T. Pointer, Effects of volcano topography on seismic broad-band waveforms, *Geophys. J. Int.*, *143*, 239–248, 2000.

Neuberg, J., R. Luckett, M. Ripepe, and T. Braun, Highlights from a seismic broadband array on Stromboli volcano, *Geophys. Res. Lett.*, *21*, 749–752, 1994.

Nuttli, O., The effect of the Earth's surface on the *S* wave particle motion, *Bull. Seismol. Soc. Am.*, *51*, 237–246, 1961.

Nuttli, O., and J. D. Whitmore, An observational determination of the variation of the angle of incidence of *P* waves with epicentral distance, *Bull. Seismol. Soc. Am.*, *51*, 269–276, 1961.

Poupinet, G., W. L. Ellsworth, and J. Fréchet, Monitoring velocity variations in the crust using earthquake doublets: An application to the Calaveras fault, California, *J. Geophys. Res.*, *89*, 5719–5731, 1984.

Saccorotti, G., and E. Del Pezzo, A probabilistic approach to the inversion of data from a seismic array and its application to volcanic signals, *Geophys. J. Int.*, *143*, 249–261, 2000.

Saccorotti, G., B. Chouet, M. Martini, and R. Scarpa, Bayesian statistics applied to the location of the source of explosions at Stromboli volcano, Italy, *Bull. Seismol. Soc. Am.*, *88*, 1099–1111, 1998.

Schmidt, R. O., Multiple emitter location and signal parameter estimation, *IEEE Trans. Antennas Propag., AP*, *34*, 276–280, 1986.

Tarantola, A., and B. Valette, Generalized nonlinear inverse problems solved using the least squares criterion, *Rev. Geophys.*, *28*, 219–232, 1982a.

Tarantola, A., and B. Valette, Inverse problems = Quest for information, *J. Geophys.*, *50*, 159–170, 1982b.

Yamaoka, K., J. Oikawa, and Y. Ida, An isotropic source of volcanic tremor-Observation with a dense seismic array at Izu-Oshima volcano, Japan, *J. Volcanol. Geotherm. Res.*, *47*, 329–336, 1991.

P. Lesage, J.-P. Métaxian, and B. Valette, Laboratoire de Géophysique Interne et Tectonophysique, Université de Savoie, F-73376 Le Bourget-du-Lac, France. (metaxian@univ-savoie.fr; lesage@univ-savoie.fr; bvale@univ-savoie.fr)